DOE/JPL/956312-83/04
(DE83017436)

STRESS STUDIES IN EFG

Fourth Quarterly Progress Report for the Period April 1—June 30, 1983

August 15, 1983
Date Distributed

Work Performed Under Contract No. NAS-7-100-956312

Mobil Solar Energy Corporation
Waltham, Massachusetts

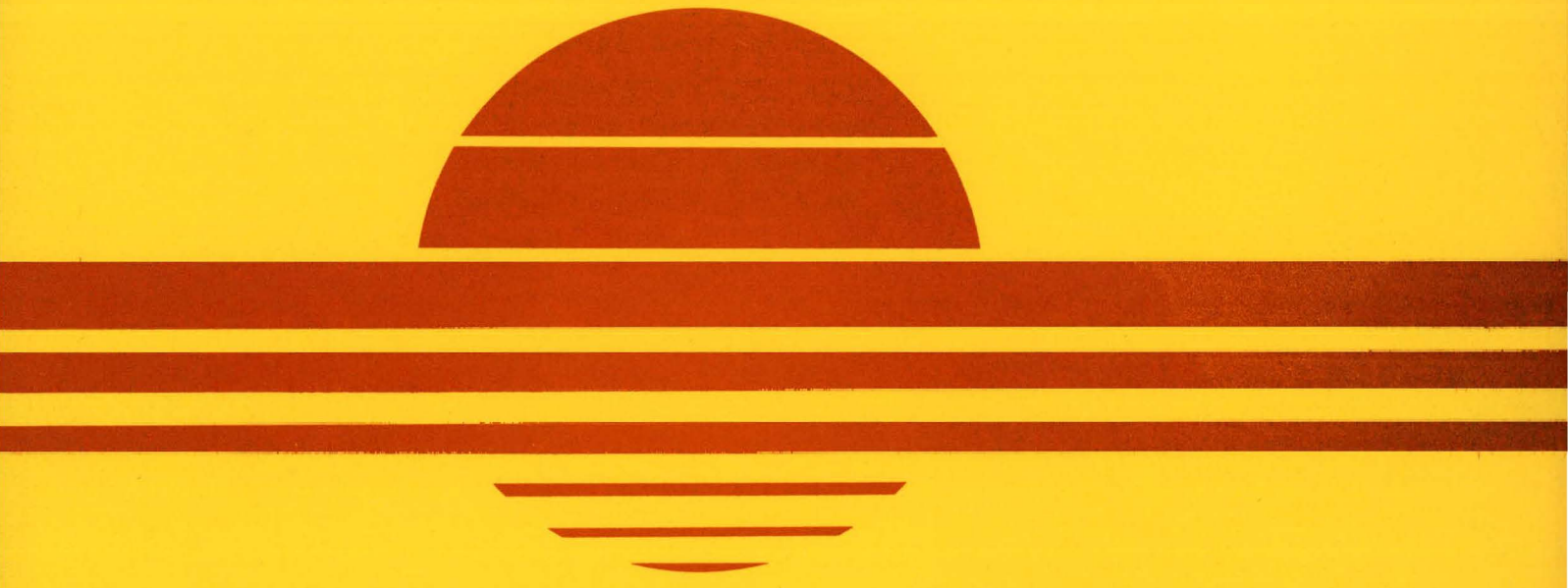

U.S. Department of Energy

Solar Energy

DISCLAIMER

DISCLAIMER

This report has been reproduced directly from the best available copy.

Available from the National Technical Information Service, U. S. Department of Commerce, Springfield, Virginia 22161.

Price: Printed Copy A04
Microfiche A01

Codes are used for pricing all publications. The code is determined by the number of pages in the publication. Information pertaining to the pricing codes can be found in the current issues of the following publications, which are generally available in most libraries: *Energy Research Abstracts (ERA); Government Reports Announcements* and Index (*GRA* and I); *Scientific and Technical Abstract Reports (STAR);* and publication NTIS-PR-360 available from NTIS at the above address.

DOE/JPL/956312-83/04
(DE83017436)
Distribution Category UC-63b

Mobil Solar Energy Corporation
16 Hickory Drive
Waltham, Massachusetts 02254

STRESS STUDIES IN EFG

Program Manager: Juris P. Kalejs

Fourth Quarterly Progress Report - Subcontract No. 956312

Covering Period: April 1, 1983 - June 30, 1983

Distribution Date: August 15, 1983

THIS PAGE

WAS INTENTIONALLY

LEFT BLANK

ABSTRACT

Stress distributions have been calculated for a creep law predicting a higher rate of plastic deformation than modeled in earlier studies. The expected reduction in stresses is obtained, although quantitative results are not yet available because of difficulties in obtaining convergent solutions.

Improved schemes for calculating growth system temperature distributions are being evaluated in a new subtask started at MIT. Other work in temperature field modeling has examined the possibility of using horizontal temperature gradients to influence stress distributions in ribbon.

The defect structure of 10 cm wide ribbon grown in the cartridge system has been examined. A new feature is identified from an examination of cross-sectional micrographs. It consists of high density dislocation bands extending through the ribbon thickness. A four-point bending apparatus has been constructed for high temperature ($\geq$ 1000°C) study of the creep response of silicon, and will be used to generate defects for comparison with as-grown defects in ribbon.

Another subtask has been started in collaboration with the University of Illinois which will examine the feasibility of laser interferometric techniques for sheet residual stress distribution measurement.

The mathematical formalism for calculating residual stress from changes in surface topology caused by an applied stress in a rectangular specimen has been developed, and the system for laser interferometric measurement to obtain surface topology data has been successfully tested on CZ silicon.

Testing and calibration of different fiber optics temperature sensor configurations are underway.

"The JPL Flat Plate Solar Array Project is sponsored by the U.S. Department of Energy and forms part of the Solar Photovoltaic Conversion program to initiate a major effort toward the development of flat plate solar arrays. This work was performed for the Jet Propulsion Laboratory, California Institute of Technology by agreement between NASA and DOE."

THIS PAGE

WAS INTENTIONALLY

LEFT BLANK

TABLE OF CONTENTS

List of Figures

I. INTRODUCTION

A satisfactory model that can account for stresses generated in silicon sheet grown at high speeds is not yet available. Numerous attempts to calculate residual stresses have been made, but all of these suffer from inadequacies in one area or another. This report describes the work in progress under this subcontract to attempt to develop and test in the laboratory a stress-temperature field model for silicon ribbon EFG. In one subtask, a computer code to predict stress-temperature field relationships in steady-state sheet growth is being developed at Harvard University. The stress state is parameterized by a two-dimensional temperature field and growth speed. Incorporation of time dependent stress relaxation effects is through a creep law to model the impact of plastic flow on the sheet residual stress state. A second aspect of the program deals with the development of a model to predict the temperature field in a moving sheet from given system component temperatures (i.e., the sheet environment), and studies experimental means to verify the model.

The results from modeling of stress in silicon sheet with creep show that plastic deformation processes can significantly reduce stress during steady-state high speed sheet growth. The initial attempts to compare calculated stress distributions and experimental results in the case of growth in the 10 cm EFG cartridge system raise a number of important issues. These relate to the directions for future research needed to provide a test for the model and information relevant for achieving reduced stress growth configurations in practice. These issues are examined here.

The initial analysis has investigated the impact of two levels of creep intensity. The creep response has been approximated by choosing a single exponent (n = 5) for the stress dependence of the strain rate and a temperature independent activation energy (~5 eV) for defect motion. This has its limitations, as evidenced by data from various workers, which show that these two parameters are a strong function of stress magnitude and of temperature. In a second approximation, only steady-state creep has been modeled, and transient effects neglected. In view of these approximations, it is not possible to choose a representative experimental datum point for a fit of the constitutive law used, as has been done up until now, and expect to arrive at an understanding of creep influence and at a test of the model at a quantitative level. Additional data on creep response relevant to silicon sheet growth are required to gain understanding both of the effect of impurities, such as carbon, on defect generation and motion in ribbon at high temperatures, and of relaxation phenomena at the stress and strain rate levels estimated on the basis of the present calculations. A program on study of high temperature creep has been started to provide more information in these areas.

The sheet temperature profiles used in the stress analysis to date all lead to large elastic stresses, sufficient to result in buckling and ribbon fracture. This includes the profile calculated for ribbon grown in the 10 cm EFG cartridge system. The residual (room temperature) stress calculated with creep included is sensitive to the details of the temperature profile in the active afterheater region of the cartridge. However, the stresses within about 5 mm of the growth interface, associated here with high temperature buckling, do not vary significantly and are not reduced appreciably for the modifications in the cartridge temperature profile examined. Attempts to vary growth conditions in

the cartridge in order to produce ribbon with different stress levels to provide a test of the model have met with limited success. They show that the 10 cm cartridge generally lacks the flexibility necessary for this work. Consideration is being given to design of a ribbon growth system more suitable for this purpose.

Calculated sheet temperature profiles have not yet been confirmed by measurements in the ribbon. Development of a temperature sensor based on fiber optics, which has the potential to provide data at a necessary level of accuracy, is in progress. This confirmation of calculated profiles is desirable because details of the heat transfer in the crucial region near the growth interface need to be ascertained. The modeling shows that the temperature profile shape is very sensitive to values used for several silicon material parameters that are not well known. This adds an uncertainty to the validity of the calculations beyond what arises from approximations used in the heat transport model. Refinement of the temperature profile calculations is in progress through application of more advanced finite element schemes for modeling of heat transport in the meniscus melt and ribbon.

Average residual stress levels have been estimated in 10 cm wide ribbon grown with several different temperature profiles using a scribe and split technique. These are found to be in the range of 10 to 30 MPa, and generally are an order of magnitude or more below the maximum predicted sheet elastic stress. The modeling shows these low measured stress levels will only be achieved through creep. The technique used cannot provide information on the stress distribution in the ribbon. Several other approaches for measuring stress are being evaluated. These include multi-finger cutting and the use of laser interferometry. An improvement in the sensitivity of the stress measurement

technique is particularly necessary in order to evaluate the impact of edge effects on the overall stress distribution. These arise from thickness nonuniformity at the ribbon edge, created primarily by growth from bulbous dies used to enhance edge stability. Deviations in both residual stress distribution and high temperature creep and buckling from those predicted for a uniform thickness ribbon can be expected to arise.

The goal of the program is to combine the results of the above areas of study to arrive at a model that can predict stress-temperature field relationships in steady-state silicon sheet growth under realistic conditions. Minimum stress configurations will be sought, and an attempt to construct an EFG silicon ribbon growth system that can verify this model will be made if it appears such configurations can be achieved experimentally.

II. PROGRESS REPORT

The experimental work on this program has been restructured into four subtasks (see also the revised Program Plan in Appendix I): (A) Advanced System Design, (B) Creep Law Studies, (C) Optical Fiber Temperature Sensor Studies, and (D) Residual Stress Measurements. The theoretical work on stress analysis will continue to study reduced stress configurations in coordination with subtask (A) above.

Work in progress in these areas is described in detail below.

A. Advanced System Design

1. Stress Analysis (J.W. Hutchinson and J.C. Lambropoulos, Harvard University)

Calculations of stress distributions have been carried out to investigate the effect of changes in the constitutive relation for creep from that used in earlier studies. This is obtained from new experimental data,[1] which give a strain rate dependence on stress and temperature considerably different from that used in the stress analysis up to this time. This relation is obtained from work hardening data taken between 1000°C and 1300°C, and encompasses higher ($\sim 10^{-2}$ s^{-1}) strain rates than used in earlier studies.

The new creep law has the form:

$$\dot{\varepsilon}^{C}_{ij} = Cf(T)\ (\sigma_e/\mu)^{n-1}\ S_{ij}$$

with $C = 5.85 \times 10^{22}$ $(GPa\text{-}s)^{-1}$, $f(T) = [\exp(-41800/T)/T]$, and $n = 3.6$. Calculations have been carried out for a speed of 6 cm/min for the cartridge system temperature profile. The results of the calculations are shown in Figs. 1 to 3. Complete convergence of the solutions was not obtained, and so the results

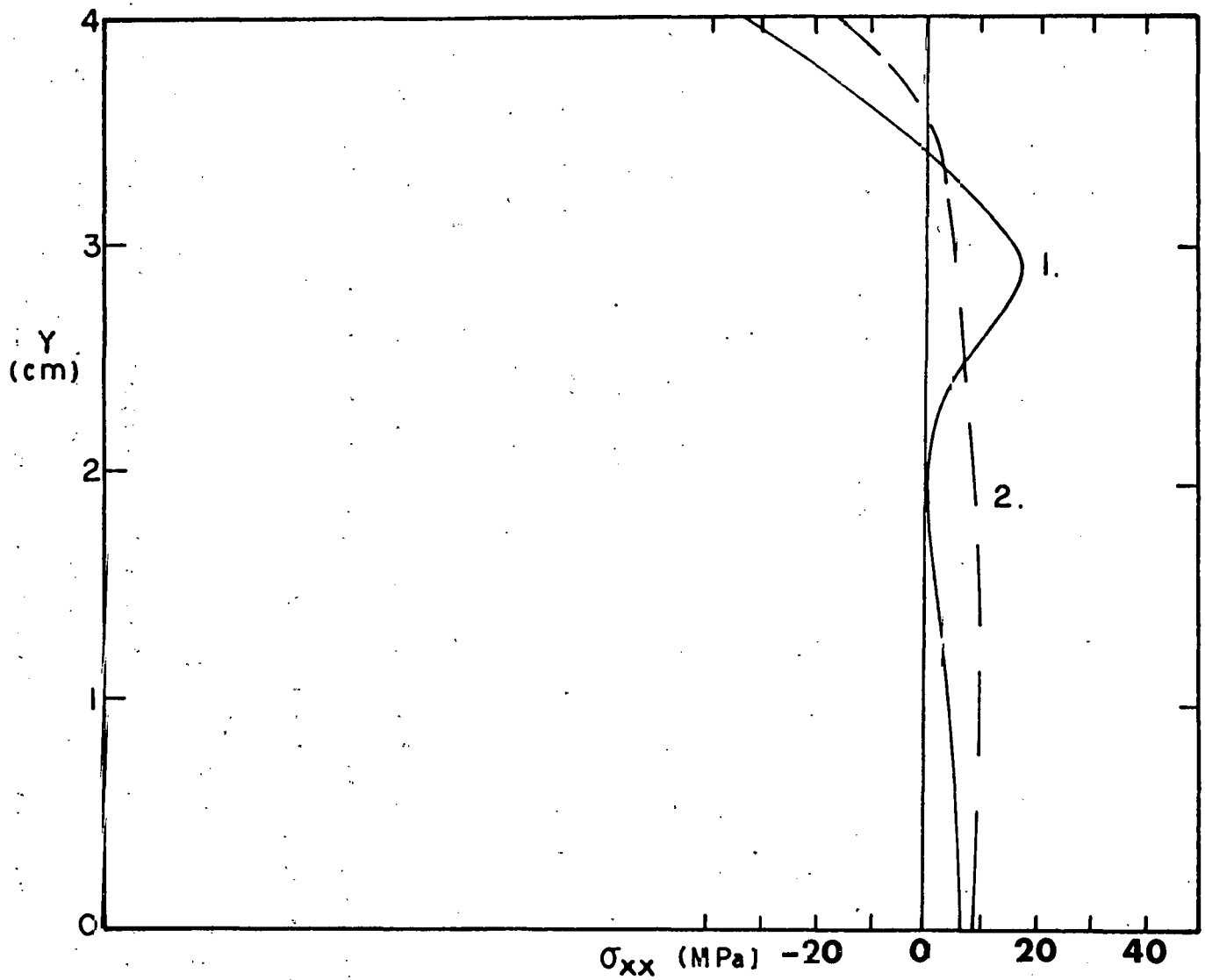

Fig. 1. Comparison of σ_{xx} variations across ribbon width at room temperature (x = 20 cm) at V = 6 cm/min for two creep laws: 1. High creep cordition, 2. new creep law.

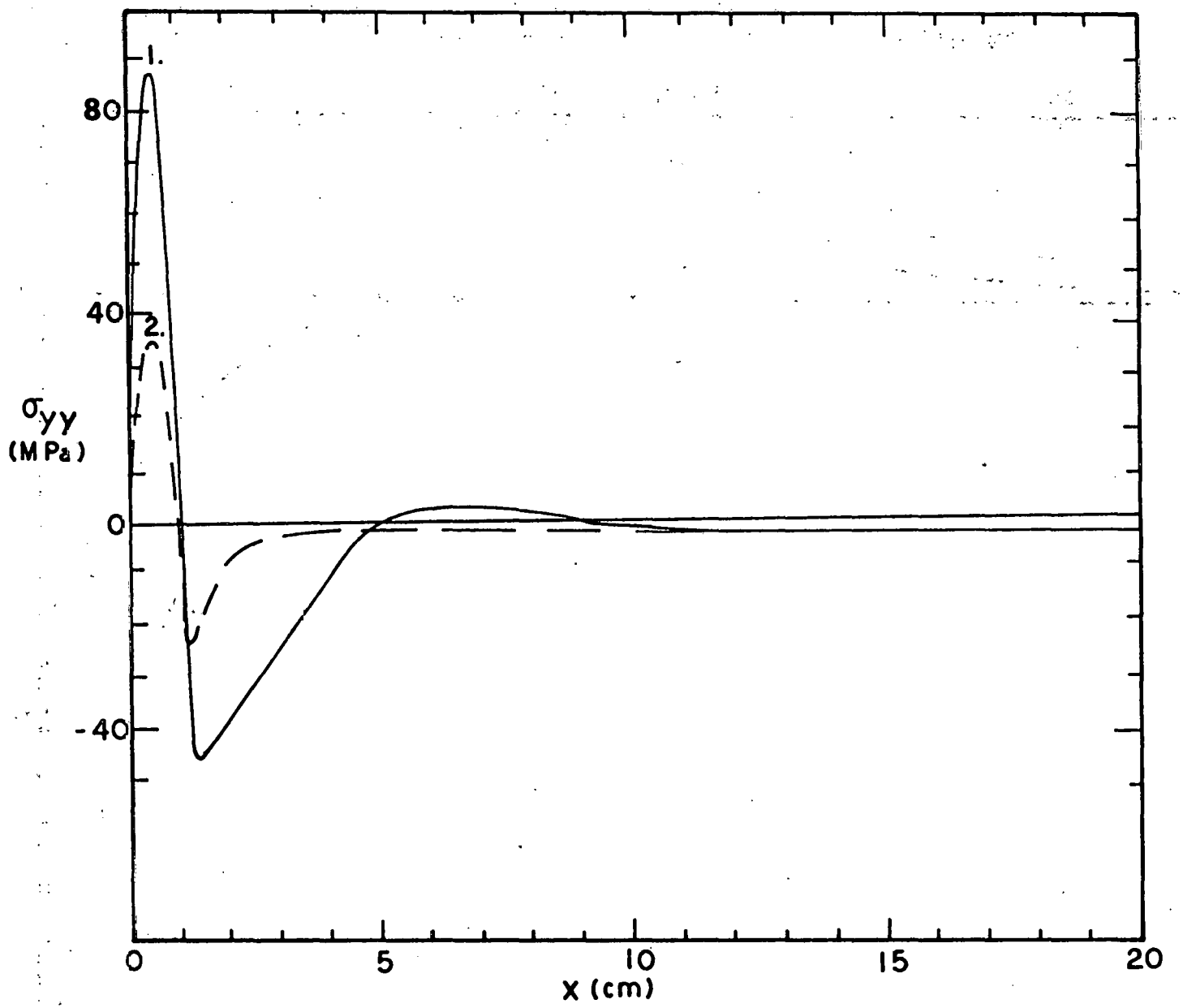

Fig. 2. Comparison of σ_{yy} along ribbon centerline at V = 6 cm/min for: 1. high creep condition, 2. new creep law.

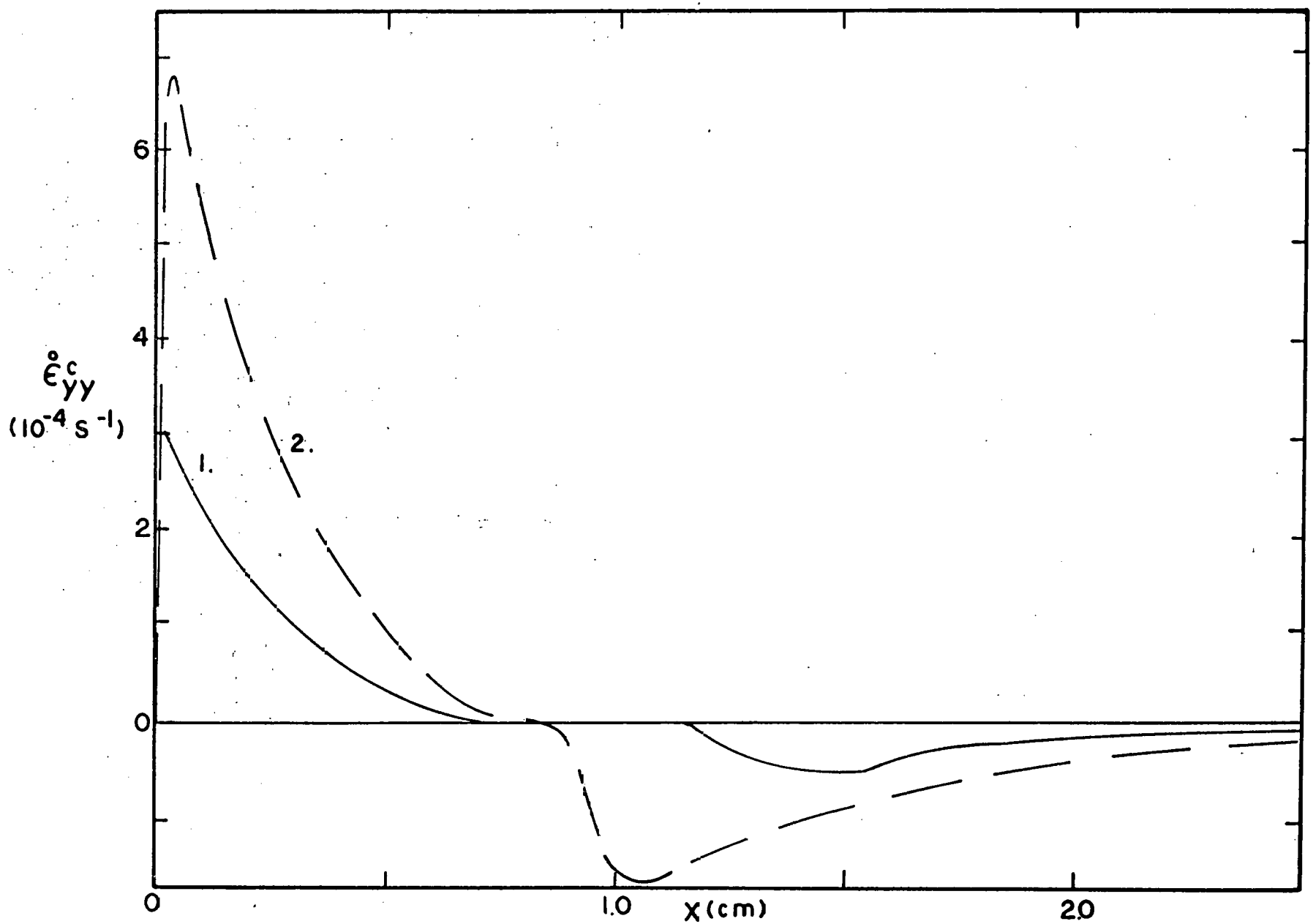

Fig. 3. Comparison of $\dot{\epsilon}^c_{yy}$ along ribbon centerline at V = 6 cm/min for: 1. high creep condition, 2. new creep law.

can only be viewed on a qualitative level. This was due to an inadequacy in the grid spacing in the region of high strain rates near the interface. The calculation grid will have to be reworked in order to eliminate this problem.

Reductions in σ_{yy} and σ_{xx} both occur, as expected, with this new constitutive relation, which predicts higher strain rates (Fig. 3) than found for even the "high" creep condition studies in our initial analysis. σ_{yy} has its peak values reduced about a factor of two, and the room temperature stress values also are reduced by about a factor of two. The distribution of the latter across the ribbon width has a central region of tensile stresses which gradually decreases and becomes compressive at the ribbon edge (Fig. 2). At levels of 10 MPa, the room temperature stresses are comparable to those estimated by applying the scribe and split technique to 10 cm wide ribbon grown with the cartridge system modeled. The peak strain rates are factors of two greater (Fig. 3) and significant regions of non-zero strain extend to the lower temperature region of the afterheater.

2. Heat Transfer Modeling (R.A. Brown and H.M. Ettouney, MIT)

Finite element analysis of the simultaneous effects of heat transfer and capillarity has extended previous work[2] to incorporate an efficient Newton iteration scheme and to include the details of the fluid flow in the melt. The Newton scheme lead to a factor of three savings in calculation time and to the implementation of computer-aided methods for tracking solution families in terms of a given parameter, e.g., growth velocity V_g, set-point temperature $\tilde{T}_o$ or static head $\tilde{h}_{eff}$. New operating limits for increasing the static head are predicted. These calculations are very significant. When taken together with those reported in Ettouney et al.[2] the finite element analysis describes the "operating region" in (V_g, T_o, $\tilde{h}_{eff}$) space for a particular die geometry and

ambient heat transfer environment. Expressing the operating limits as $V_g = V_g(\tilde{T}_o, \tilde{h}_{eff})$ gives the maximum accessible growth velocity for any particular combination of $\tilde{T}_o$ and $\tilde{h}_{eff}$. We are exploring now the effect of changes in capillary width on this growth rate ceiling.

A direct comparison has been completed between calculations which include the details of the velocity field in the melt and ones using a modified uniform velocity field that accounts for the tapering of the meniscus. The two calculations were found to be in good agreement in silicon for growth speeds below 5 cm/min. The details of convective heat transfer become important in silicon only near growth speeds of 50 cm/min, but at much lower speeds for the solidification of materials with lower thermal conductivity, e.g., Al_2O_3.

A comparison between measurements of sheet thickness as a function of growth speed is being carried out. Using the ambient temperature distribution measured by Kalejs and Bell at Mobil Solar, thickness versus growth rate data[3] will be fit over the entire range of pull speed using the die set-point $\tilde{T}_o$ and die ambient $\tilde{T}_\infty$ temperatures as adjustable parameters. Of these, the die set-point value is the most important. Plans have been made for a systematic set of experiments with varying $\tilde{T}_o$, $\tilde{h}_{eff}$ and V_g for a more comprehensive check of the EFG model and the operating limits predicted by it.

3. EFG System Temperature Field Modeling (R.O. Bell and J.P. Kalejs, Mobil Solar)

It has been suggested that horizontal temperature gradients (across the ribbon width) may be used to compensate for the effects of high vertical gradients and to reduce the overall level of stress present during sheet growth. We have investigated the possibility of doing this in the 10 cm EFG system by introducing horizontal heat flux variations into the temperature field model and calculating resulting horizontal ribbon isotherms.

In most of the temperature modeling calculations, the ribbon surface heat flux has been calculated assuming that the horizontal temperature was constant across the width of the ribbon enclosure, beyond which (i.e., at the enclosure end wall) it was room temperature (300°K). Thus the flux is essentially constant until very near the ribbon edge. To simulate the effect of an enclosure wall horizontal gradient, the ribbon surface flux was assumed to decrease as if its effective temperature decreased 100°C from the center to the edge with a quadratic curvature, i.e., $T_{eff} = T_{center} - 100\ (y/W)^2$.

Figure 4 shows calculated horizontal ribbon temperatures superimposed on the profile along the center of the ribbon. In all cases the horizontal gradient is zero at the ribbon edge because of the boundary conditions. The thermal conductivity of the silicon smooths out the horizontal variations so that the largest edge to center temperature difference in the ribbon is 55°C rather than the 100°C imposed. The maximum horizontal gradient is of the order of 35°C/cm for this 300 μm thick ribbon. This is very small compared to the 1500°C/cm vertical gradients near the interface but comparable to those 3 or 4 cm from the interface.

The large interface gradients will make it difficult to tailor the horizontal temperature to compensate for stresses produced near the interface, but it might be possible to deal with stresses generated a centimeter or so away from the interface. The question still remains as to which region dominates the room temperature stress distribution. This will be strongly dependent on the creep rate and its temperature variation and on the detailed shape of the temperature profile. Creep experiments are in progress at Mobil Solar and are discussed further below.

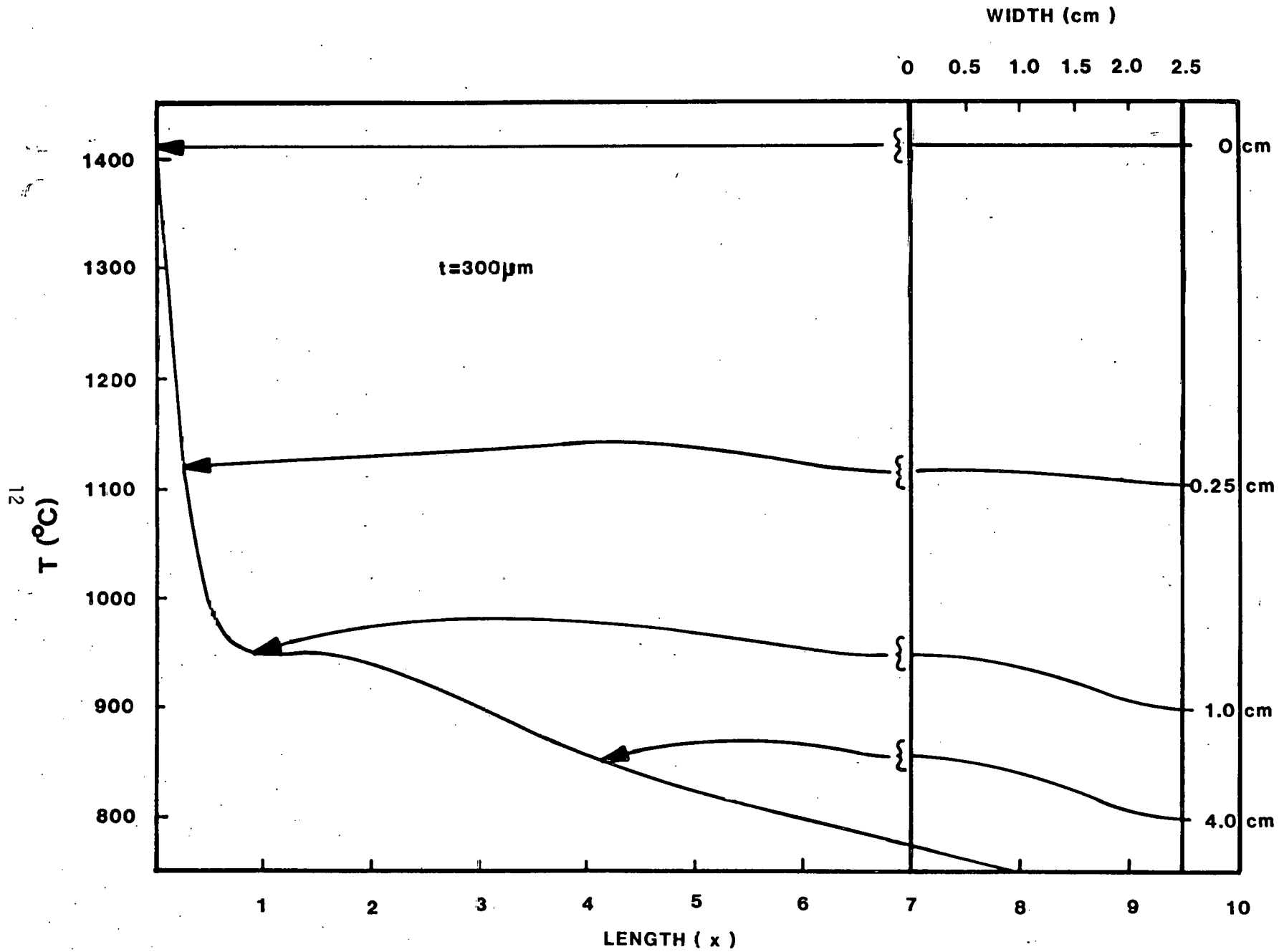

Fig. 4. Horizontal temperature variations in 300 μm thick sheet (see text for explanation).

Temperature field data were incompletely reported in the third quarterly report[4] because of the omission of one case from a table. Thus, Table II on page 16 of this report is reproduced here with a fourth case, Case D, included.

Table II. Thermal Conditions and Geometry used in Modeling.
(Corrected Table from Third Quarterly Report.)

	Curve A	B	C	D
Ribbon Thickness	300 μm	300 μm	300 μm	300 μm
Base Plate Temperature	1500°C	1200°C	1200°C	1500°C
Cold Shoe Temperature	450	450	400	400
Afterheater Temperature	1200	1200	960	960
$dT/dx\big\|_{x=0}$	1310	1370	1490	1427

On account of this omission, wrong identification of the temperature distributions used in stress calculations was made. Curve A should now correspond to the EFG profile, Case 1, and Curve D to the reduced afterheater profile, Case 3, of Fig. 1 of the third quarterly report.

B. Creep Law Studies

1. Four-Point Bending

A four-point bending apparatus has been constructed for use at high temperatures to study creep in silicon and is at present being tested. It is made of graphite in order to withstand temperatures up to the melting point of silicon, and follows fairly closely the ASTM E328 recommended apparatus. A side view of the apparatus is shown in Fig. 5.

The first experiments have been carried out on initially defect-free CZ silicon wafers and on Silso silicon. Samples were cut into approximately 5 cm by 10 cm blanks. CZ and Silso sample thicknesses were 0.3 and 0.4 mm.

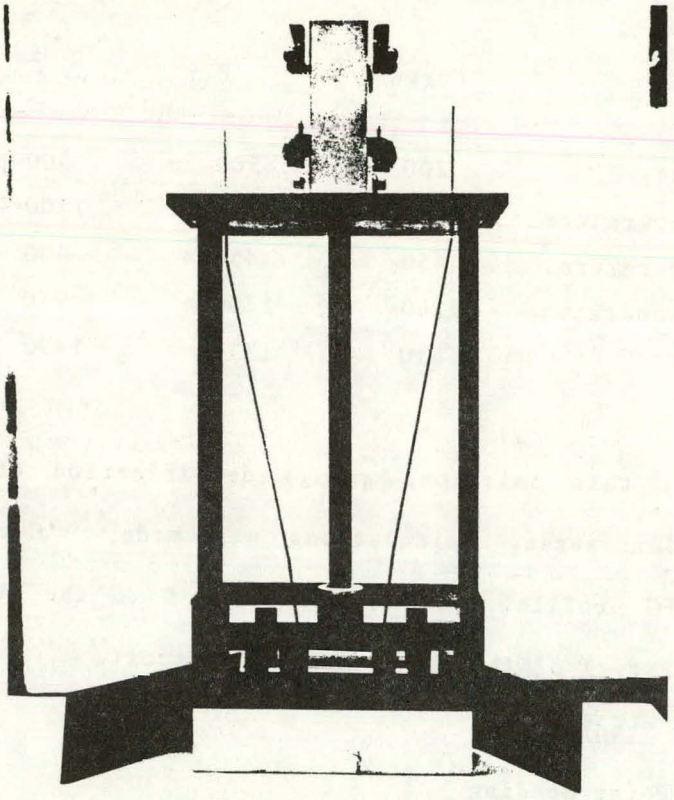

Fig. 5. Four-point bending apparatus for high temperature experiments.

Experiments have been carried out at two temperatures, 1215°C and 1360°C. The samples were stressed under progressively increasing loads until a total deflection of about 0.10 to 0.12 cm was obtained. Then the load was removed and the samples were cooled to room temperature. The displacement vs. time graphs are given in Fig. 6.

The idealized stress distributions along the sample length and through its thickness are shown in Fig. 7 for the four-point bending configuration used here. The maximum surface stress (tension on the bottom and compression on the top) is calculated from the moment of inertia I and bending moment M as:

$$\sigma_s = \frac{MC}{I}$$

$$I = \frac{1}{12} Wt^3 \qquad M = F\ell$$

For our experiments W = 5 cm and ℓ = 1.9 cm. Thus for loads of 100 to 200g, the maximum σ_s values are of the order of 10 MPa for typical sample dimensions. For the data of Fig. 6, σ_s values up to about 15 MPa were realized.

Future plans for the creep experiments are to study the defect structure generated in CZ wafers as a function of loading conditions, and to compare it to as-grown ribbon structure.

2. Ribbon Defect Studies

Ribbon cross sections have been examined to try to identify defect features and their distribution which may give information on stresses acting during ribbon growth. The ribbon was sectioned perpendicular to the growth direction, polished and etched to reveal the cross-sectional structure. Several typical micrographs are shown in Fig. 8 and 9. A new class of dislocation arrangements is shown there. These occur in the form of narrow bands of very

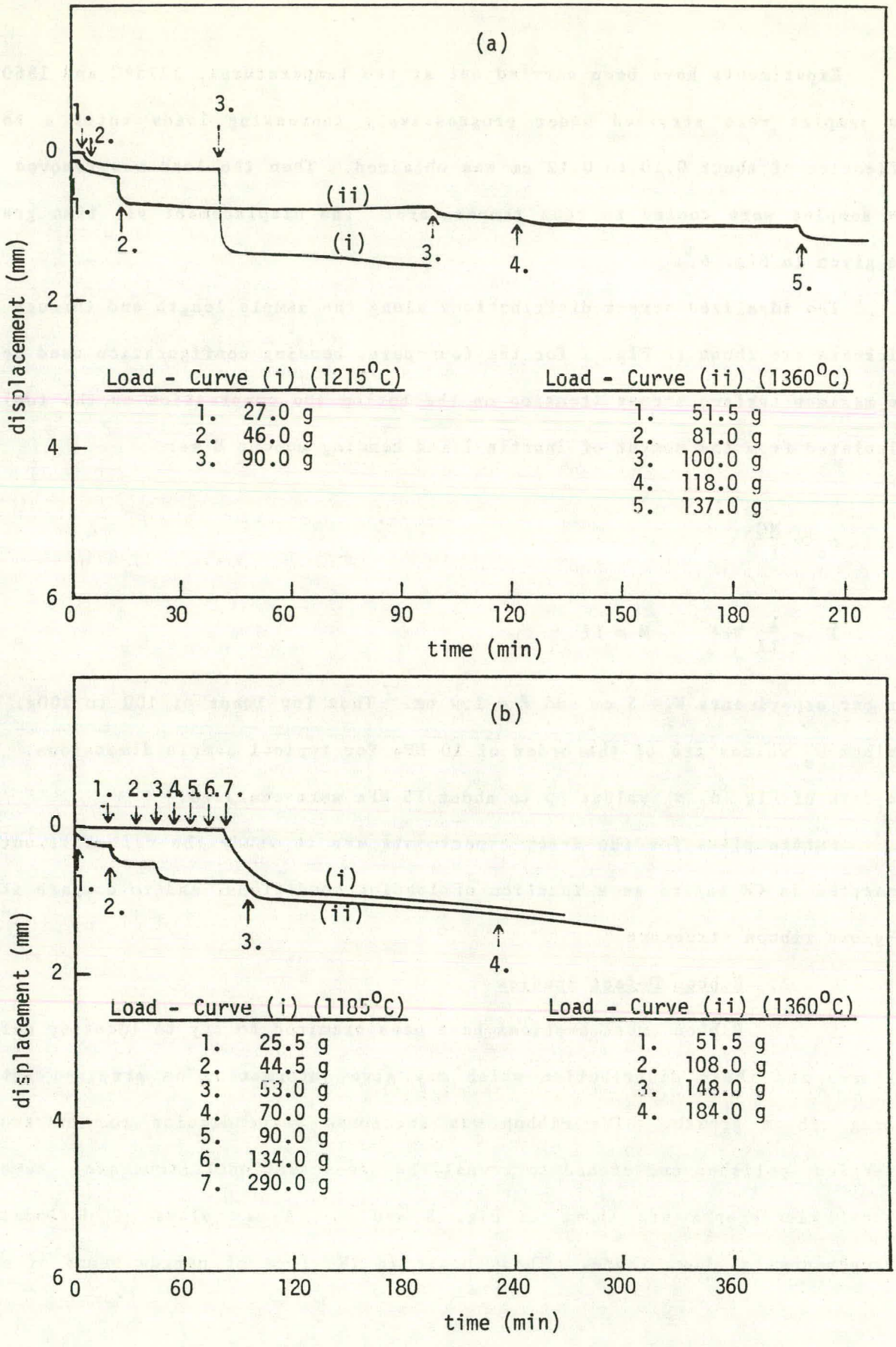

Fig. 6. Displacement vs. time graphs for (a) CZ, and (b) Silso silicon wafers stressed by four-point bending.

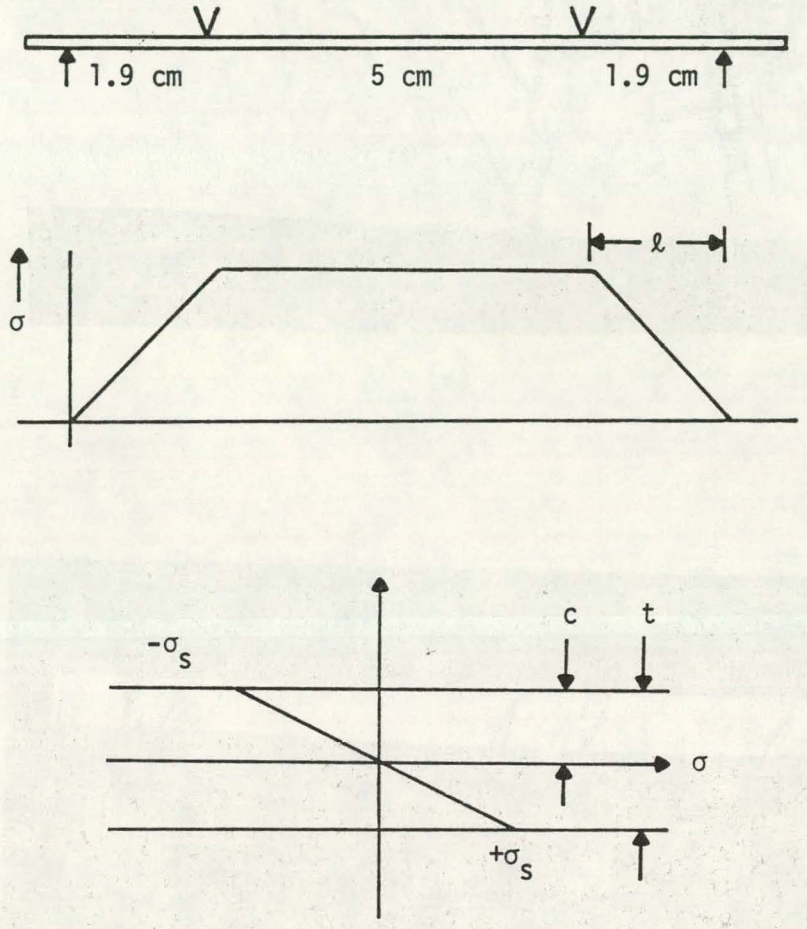

Fig. 7. Geometric and stress relationships for sample of thickness t (and c = t/2) in four-point bending.

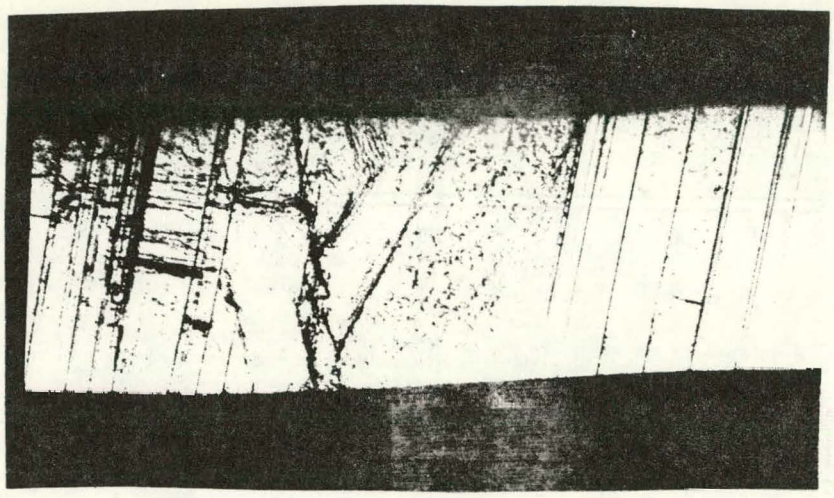

(a)

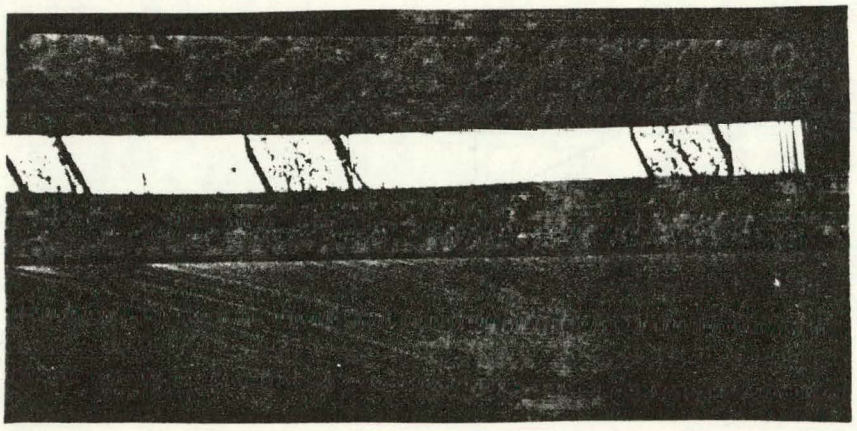

(b)

Fig. 8. Cross-sectional micrographs of 10 cm wide ribbon grown at 2.6 cm/min and with afterheater setting of 1000°C. (a) Magnification X70.4, ribbon thickness is 0.55 mm; (b) magnification X45.2, thickness 0.15 mm.

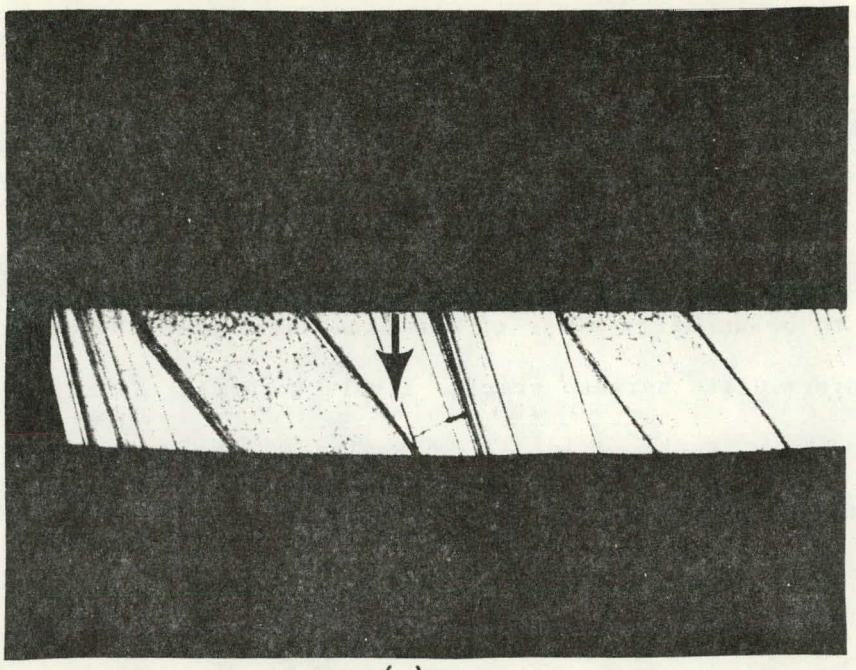

(a)

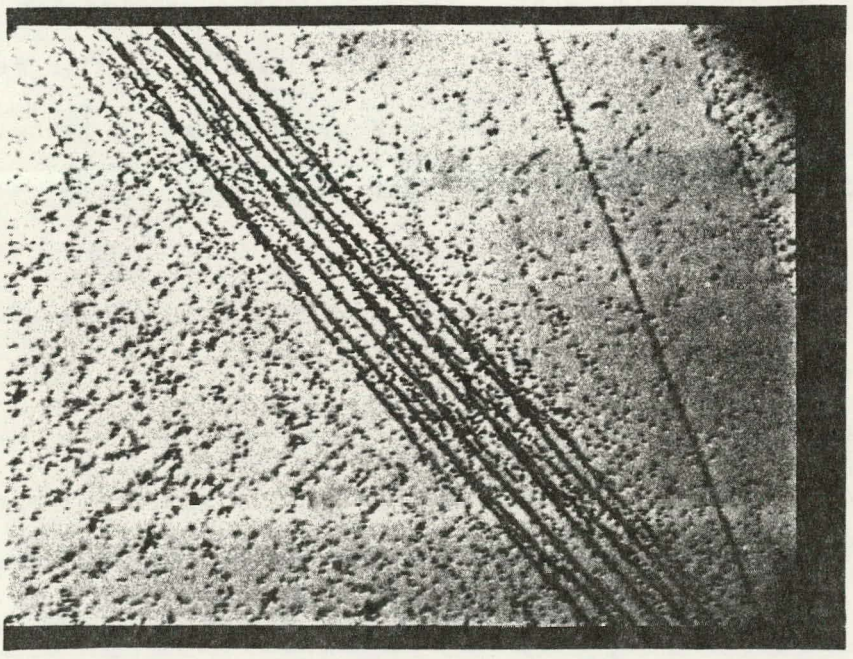

(b)

Fig. 9. Cross-sectional micrographs of 10 cm wide ribbon grown at 3.5 cm/min and afterheater setting of 1100°C. (a) Magnification is X70.4, ribbon thickness is 0.28 mm; (b) high magnification (X652) view of area identified by arrow in (a).

high dislocation density which extend through the cross section. These are typically of the order of the ribbon thickness in extent, and are bounded by what appear to be slip bands or yet more intense dislocation bands. Figure 8(a) shows what appears to be an early stage of the band development, where the dislocation density is intermediate between average levels occurring in adjacent regions and that in more highly stressed bands. Examples of the latter are found in Fig. 8(b). The bands occur often in pairs or triplets separated by distances of the order of several times the ribbon thickness. Double bands, such as shown on the right of Fig. 8(b) are also commonly observed.

A high magnification micrograph of one of the more intensely dislocated band edges is shown in Fig. 9(b). These regions do not appear to be oriented along the twin plane directions (one of which lies also in this micrograph), but rather appear to make larger angles with respect to the surface than do the typical twin planes seen in the cross sections.

C. Fiber Optics Temperature Sensor

A probe was constructed to hold the high and the low temperature portions of the fiber optics sensor in a configuration that would allow it to be placed conveniently into the afterheater region of the 10 cm cartridge. The first test of the probe in the cartridge was to measure temperature in the hottest part of the afterheater, and to use the afterheater thermocouple as a reference. Initial tests of the probe showed the signal level was much higher than that occurring in the test furnace used for the initial sensitivity studies. It was decided to go to a two wavelength measurement in order to make absolute temperature determinations and so avoid the problems associated with varying light intensity levels.

The two wavelengths chosen for the measurement were 0.6 and 0.7 μm. The probe was calibrated at room temperature with a spectral radiometer using a tungsten ELH lamp operating at a temperature of 3320°K. The afterheater region temperatures were again monitored. It was found that the probe calibration factor obtained at room temperature still did not give temperatures that corresponded to the afterheater thermocouple readings.

It appears that the major problem with the probe at present is that too much stray radiation is being accepted into the fiber optics circuit that originates from regions other than the probe tip. A second probe is being constructed that will be placed in a cooler region of the cartridge near the cold shoes to attempt to reduce the effects of stray radiation.

D. Residual Stress Measurements (A.T. Andonian and S. Danyluk, University of Illinois at Chicago)

It has recently been proposed that laser interferometry may be used to evaluate residual stress distributions on a macroscopic scale in sheets of a material such as silicon. In this technique, the laser light is used to generate surface topographs of the sheet surface under different states of applied stress, and the deformations measured are used to back calculate the residual stress in the sheet. The mathematical formation for calculating the residual stresses has been developed, and is given for a rectangular sample geometry in Appendix II. The apparatus for the topology measurement has been constructed and tested to successfully back calculate an applied in-plane stress in a CZ silicon wafer. These results are discussed in Appendix III. The next step is to attempt to measure residual stress in EFG ribbon.

REFERENCES

1. H. Siethoff and W. Schröter, Scripta Met., 17 (1983), 393.

2. H.M. Ettouney, R.A. Brown and J.P. Kalejs, J. Crystal Growth, 62 (1983), 230.

3. J.P. Kalejs, Second Quarterly Report, DOE/JPL 956312/83/02 (February 1983).

4. J.P. Kalejs, Third Quarterly Report, DOE/JPL 956312/83/03 (April 1983).

APPENDICES

1. Proposed program plan for period July 9, 1983, to July 8, 1984.

2. "Relations Between In-Plane Residual Stresses and Out-of-Plane Deflections in Silicon Ribbon Subjected to Bending", by A.T. Andonian and S. Danyluk, University of Illinois at Chicago.

3. "Residual Stress in Sheet Silicon as Determined by Laser Interferometry", by A.T. Andonian and S. Danyluk, University of Illinois at Chicago.

APPENDIX I

WORK BREAKDOWN STRUCTURE AND PROGRAM PLAN

July 9, 1983 - July 8, 1984

"STRESS STUDIES IN EFG"

Subject	Description	'84 JUL	AUG	SEP	OCT	NOV	DEC	JAN	FEB	MAR	APR	MAY	JUN	JUL
Theoretical	Modeling of reduced stress growth configurations.	X----------												----------X
Experimental	Advanced system design concept testing.				X----------									----------X
	High temperature creep measurements in silicon.	X----------					----------X							
	Temperature measurements with optical fiber systems in support of modeling.	X----------					----------X							
	Residual stress measurement technique development.	X----------					----------X							
Program Management	Progress Reports, etc.	X----------												----------X

THIS PAGE

WAS INTENTIONALLY

LEFT BLANK

APPENDIX II

RELATIONS BETWEEN IN-PLANE RESIDUAL STRESSES AND OUT-OF-PLANE DEFLECTIONS IN SILICON RIBBON SUBJECTED TO BENDING

by

A. T. Andonian and S. Danyluk

May 1983

University of Illinois at Chicago
Department of Civil Engineering, Mechanics
and Metallurgy
P.O. Box 4348
Chicago, IL 60680

ABSTRACT

Residual stresses in silicon ribbon can result from a two-dimensional temperature field or a change in the growth speed of the ribbon and the magnitude and sign across the width of the ribbon can vary. These stresses can be related analytically to an intentionally applied out-of-plane bending moment and the curvature of the distorted ribbon, quantities which can be easily obtained by a unique experimental measurement. This report is a summary of an analysis assuming two conditions on residual stresses in silicon ribbon: in-plane tension and side shear and in-plane compression and side shear.

INTRODUCTION

Residual stresses are extremely important in silicon ribbon since these stresses can cause buckling and in some cases fracture of the ribbon. A knowledge of the magnitude and sign of the residual stresses can therefore be used to optimize the growth conditions of silicon ribbon. However, at present, our knowledge of residual stresss in silicon ribbon is sketchy. Some recent modeling has shown [10] that thermal gradients and change in growth speed of the ribbon can result in non-uniform residual stresses across the width of the ribbon. Experiments are underway to verify these stresses but these experiments are destructive.

Several non-destructive techniques are available for determining residual stresses. The two most widely used are the X-ray technique and the hole-drilling strain gauge method [1-7]. Both techniques have limitations. The X-ray technique is limited since X-ray absorption occurs within several micrometers of the surface depth. The resolution of this technique is

$\sim$ 5 ksi over several mm^2 in area. In addition, stresses throughout the thickness cannot be determined conveniently. Another technique is the hole-drilling strain gauge method where a special rosette strain gauge is bonded to the ribbon and connected to a strain measuring instrument. A small hole is then drilled through the center of the gauge and the resulting change in strain around the hole due to relaxation is measured. This technique is semi-destructive and measures the strains within the top surface layers (usually a few millimeters) and a very specific location. A determination of stresses is obtained from the strains. Both techniques are unsatisfactory for measuring residual stresses in ribbon because (1) the thickness of silicon ribbon is $\sim$1 mm or less and stresses through the thickness are desired and (2) residual stresses over a large area are needed.

Residual stresses can be determined by double beam interferometry which relies on the application of flexural loads and the measurement of the deflection and curvature of the silicon ribbon. Out-of-plane deflection will either be accentuated or reduced depending on the sign and magnitude of the residual stresses. The residual stresses are then determined by comparing the measured and predicted deflections and curvature. Any difference is ascribed to residual stress.

This technique has a number of advantages over existing non-destructive techniques for the measurement of residual stresses [1-7]. First, large spatial areas can be examined in contrast to the X-ray or blind hole drilling techniques. Second, through-the-thickness measurements are made as opposed to only the top surface layers as in the other mentioned techniques. One disadvantage is that the residual stresses may vary significantly through-the-thickness and the interferometry technique will average these values.

In this progress report, we present the analysis for the relationship between the deflection and curvature and the bending moment and residual stress in thin rectangular ribbon. This analysis will be used in conjunction with experimental measurements on determining the residual stresses.

ANALYSIS

We make use of a stress analysis by Hutchinson and Lambropoulos [10] of steady-state ribbon growth. Their model takes into account a two-dimensional temperature field and steady state growth conditions of the ribbon. After cooling, the stress conditions are

$$-30 \text{ MPA} < \sigma = f(y) < 30 \text{ MPa}$$

where x is in the direction of ribbon growth and y is along the width.

Figure 1 shows typical residual stress variation along the width of the silicon ribbon representative of those found [10]. Due to the heterogeneous nature of σ, residual shear stresses will be produced in the x-y plane. An analysis of the residual stresses in the ribbon must include the tensile, compressive and shear stresses in the ribbon. Figure 2 shows qualitatively the variation of shear flow, q, along a longitudinal section (parallel to x-y plane). This variation in 'q' can be assumed to be linear except at the end sections where the shear stress should be zero since the ends of the ribbon are traction free. The assumed variation in shear flow shown in Fig. 3 can be expressed as

$$q \simeq K\left(\frac{L}{2} - x\right) \tag{1}$$

where K represents the change in shear flow per unit length.

The variation of σ_x along the width identified in Fig. 2 necessitates the use of separate models for different states of stress. Formulations for two different cases are presented in the following sequel.

Case I: Rectangular Plate Under Bending, In-Plane Tension and Side Shear

If the ribbon shown in Fig. 2 was subjected to an out-of-plane bending, the mid-portion could be treated as a rectangular plate under bending, in-plane tension and side shear. The state of loading for a narrow strip of width Δy is shown in Fig. 4.

If the deflection along the ribbon is approximately as

$$w = Ax^2 + Bx + C$$

and the boundary conditions are given as

$$[x = 0, \quad w = 0]$$

$$[x = L, \quad w = 0]$$

then

$$w = A(x^2 - Lx) \tag{2}$$

Considering angular equilibrium,

$$M' = M - Pw + M_q \tag{3}$$

where

$$M_q = 2 \int_0^{x_o} qw \, dx \tag{4}$$

From linear equilibrium the stress residual in the x-direction can be written as

$$P = 2 \int_0^{x_o} q \, dx \tag{5}$$

substituting Eq. (1) into Eq. (5)

$$P = 2 \int_0^{x_o} K\left(\frac{L}{2} - x\right) dx$$

solving for K

$$K = \frac{P}{Lx_o - x_o^2} \tag{6}$$

and comparing Eqs. (1) and (6) we get

$$q = \frac{P}{x_o^2 - Lx_o} \left(x - \frac{L}{2}\right) \tag{7}$$

Substituting Eqs. (9) and (7) into Eq. (11)

$$M_q = 2 \int_0^{x_o} \left(\frac{P}{x_o^2 - Lx_o}\right)\left(X - \frac{L}{2}\right) A\left(x^2 - Lx\right) dx$$

or

$$M_q = \frac{AP}{2}\left(x_o^2 - Lx_o\right) \tag{8}$$

Substituting Eq. (8) into Eq. (3)

$$M' = M - Pw + \frac{AP}{2}\left(x_o^2 - Lx_o\right) \tag{9}$$

Finally assuming small deflections and utilizing the relation for plate curvature, we get

$$\frac{1}{\rho} = \frac{d^2w}{dx^2} = -\frac{M'}{D}$$

where

$$D = \frac{Eh^3b}{12(1-\nu^2)}$$

h = plate thickness

b = plate width

E = modulus of elasticity

ν = Poisson's ratio

The governing equation for Case I can then be written as

$$\frac{d^2w}{dx^2} = -\frac{M}{D} + \frac{P}{D}w - \frac{AP}{2}\left(x_o^2 - Lx_o\right) \tag{10}$$

where

$$\frac{d^2w}{dx^2} = 2A \quad \text{(to be determined experimentally)}$$

M = applied moment (known)

w = measured deflection at x_o

Next a portion of the ribbon subjected to compressive residual stresses (between A and C or G and I) will be considered.

Case II: Rectangular Plate Under Bending, In-Plane Compression and Side Shear

The state of loading for this particular case is shown in Fig. 5. Similar to Case I, the angular equilibrium can be expressed as

$$M' = M + Pw - M_q \tag{11}$$

Substituting Eq. (8) into Eq. (11)

$$M' = M + Pw - \frac{AP}{2}\left(x_o^2 - Lx_o\right) \tag{12}$$

and the governing equation

$$\frac{d^2w}{dx^2} = -\frac{M}{D} - \frac{P}{D}w + \frac{AP}{2}\left(x_o^2 - Lx_o\right) \tag{13}$$

As can be seen from Eqs. (10) and (13), the curvature at any length along a deflected ribbon is dependent on M, the applied moment and P, the stress residual.

To determine the distribution of residual stresses a moment is applied and the deflection is recorded. A parabolic curve fitting procedure is then used to fair parabolas through a series of data points along x and y axes in order to find the slope and curvature of the deflected surface at desired locations. Finally, experimentally-computed values of slope and deflection can be used in the theoretical model presented here to find the in-plane residual stress distribution.

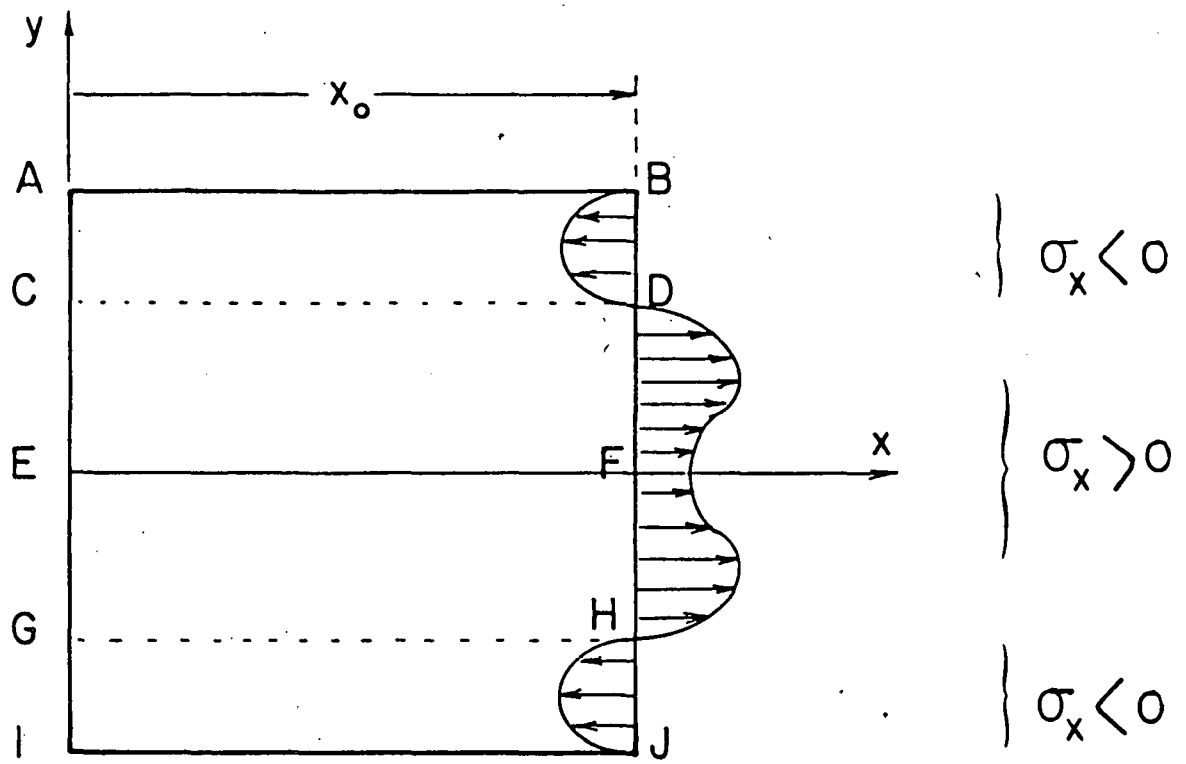

Fig. 1. Schematic representation of residual stresses along an arbitrary transverse section of a silicon ribbon.

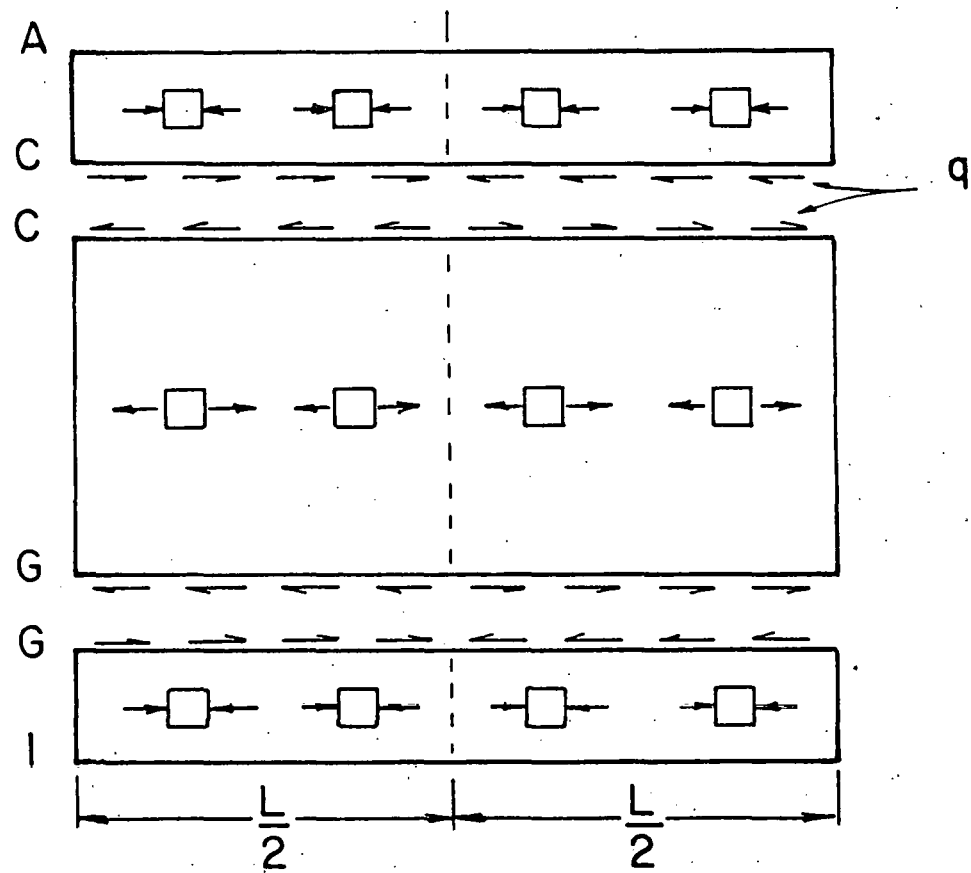

Fig. 2. A schematic representation of the residual stresses along the length of a silicon ribbon and the shear flow on longitudinal sections where the sign of residual stress changes.

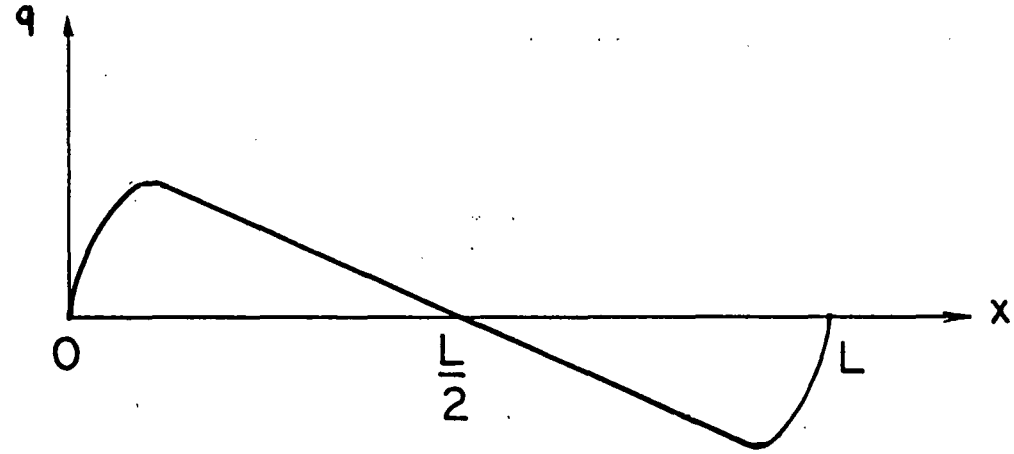

Fig. 3 Shear flow variation along a longitudinal cut in a silicon ribbon.

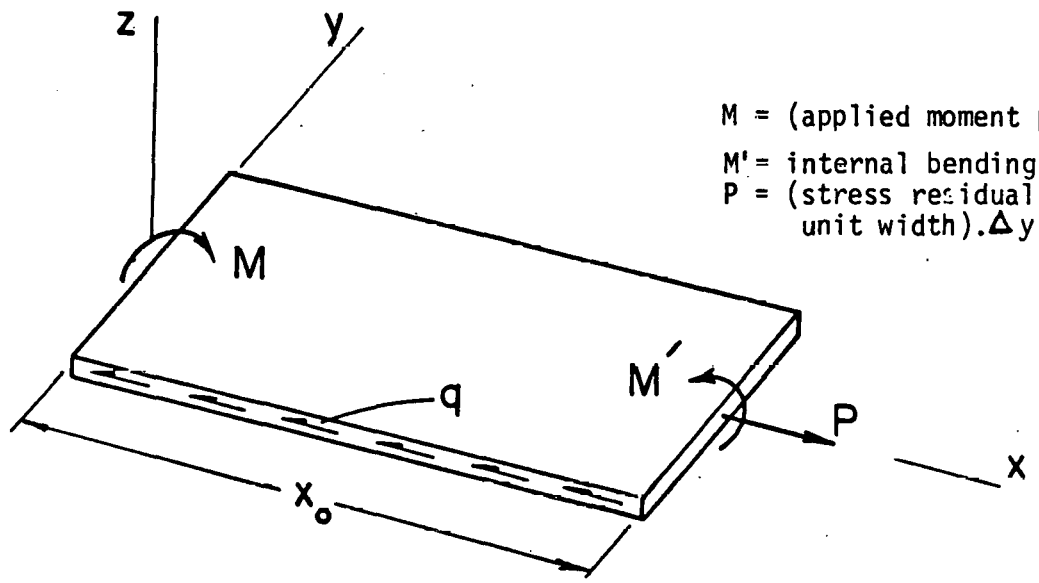

M = (applied moment per unit length).Δy

M' = internal bending moment at x_o.

P = (stress residual along x per unit width).Δy

Fig. 4 State of loading in Case I.

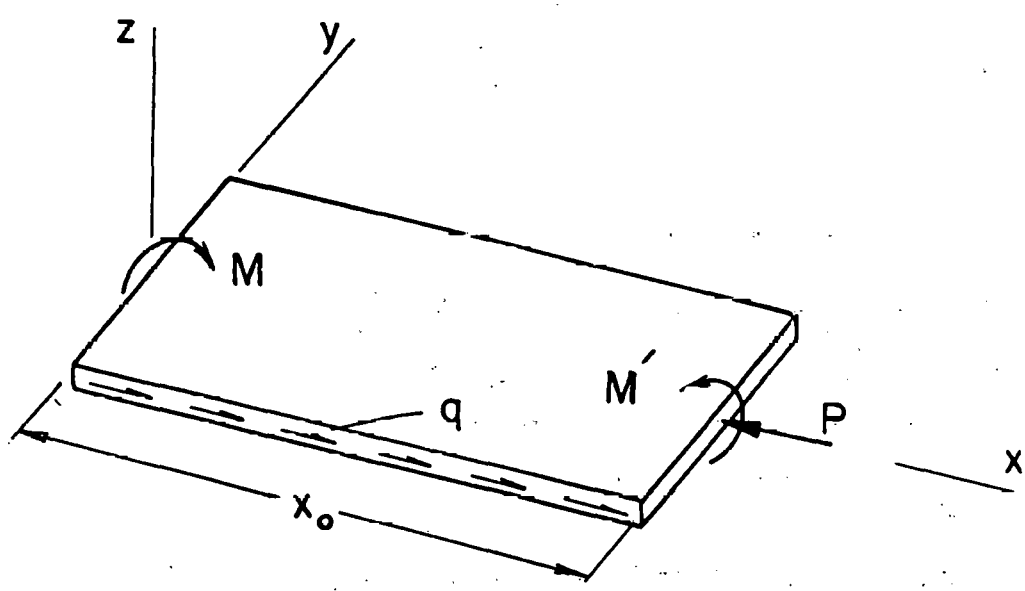

Fig. 5 State of stress in Case II.
(M, M', P are as described in Fig.4)

REFERENCES

[1] J.T. Norton, "X-Ray Determination of Residual Stress", Materials Evaluation, 31, 1973, 21-24.

[2] M. James and J.B. Cohen, "PARS, A Portable X-Ray Analyzer for Residual Stresses", ASTM J. of Testing and Evaluation, 6 (2), 1978, 91-97.

[3] R.G. Bathgate, "Measurement of Non-Uniform Biaxial Residual Stresses by the Hole-Drilling Method", Strain J. of BSSM, 4 (2), 1968, 20-29.

[4] H. Fukuoka, H. Toda and H. Naka, "Nondestructive Residual-Stress Measurement in a Wide-Flanged Rolled Beam by Acoustoelasticity", Exp. Mech., 23 (1), 120-128.

[5] V. Wilhelmy and H. Kubler, "Probe for Measurement of Strains Inside Solid Bodies", Proc. of SESA, 30 (1), 1973, 142-144.

[6] J.H. Underwood, "Residual Stress Measurement Using Surface Displacements Around an Indentation", Proc. of SESA, 30 (2), 1973, 373-380.

[7] N. Tebedge, G. Alpsten and L. Tall, "Residual-Stress Measurement by the Sectioning Method", Proc. of SESA, 30 (1), 1973, 88-96.

[8] Experimental Techniques in Fracture Mechanics, SESA Monograph No. 2, ed., A.S. Kobayashi, Iowa State University Press and Society for Experimental Stress Analysis Publ., Westport, Conn., 1975.

[9] Holographic Interferometry, C.M. Vest, John Wiley and Sons, Inc. Publ., 1979.

[10] J.P. Kalejs et al., Second Quarterly Report, DOE/JPL 956312/83/02 (February 1983).

THIS PAGE

WAS INTENTIONALLY

LEFT BLANK

APPENDIX III

Residual Stress in Sheet Silicon as Determined by Laser Interferometry*

by

Arsavir T. Andonian

and

Steven Danyluk

Department of Civil Engineering

Mechanics and Metallurgy

University of Illinois at Chicago

July 1983

* Work supported by the Mobil Solar Energy Corporation and the Jet Propulsion Laboratory-Flat Plate Solar Array Project.

ABSTRACT

As laser interferometry technique is used to determine deflections of single crystal sheet silicon to an accuracy of 316 nm. These deflections are utilized with an analysis to yield the silicon through-thickness residual stresses. The sensitivity of the technique to extract residual stresses has been determined by application of in-plane loads that simulate the residual stresses and using the plate deflection and our theoretical analysis to calculate the in-plane loads. The calculated and applied in-plane loads corresponded to within 8% for stresses of the order of 100 kPa (14 psi).

INTRODUCTION

Residual stresses are extremely important in silicon ribbon since these stresses can cause buckling and in some cases fracture. The importance of these stresses has been ellucidated in previous reports, and a number of workers are attempting to calculate and measure these residual stresses as a function of growth parameters of the ribbon. We are experimenting with a laser interferometry (non-destructive) technique that utilizes a conventional laser interferometry apparatus in conjunction with a novel loading geometry and analysis to extract residual stresses in thin silicon sheet. Since the technique is new, we have attempted to determine its sensitivity by testing rectangular-shaped single crystal Czochralski silicon whose residual stresses are assumed to be zero. We have applied in-plane loads which simulate residual stresses and we have used the experimental data and analysis to extract these loads.

EXPERIMENTS

A block diagram of the essential elements of the technique and a schematic of the experiment are shown in Figs. 1 and 2. A single crystal - 0.6 mm thick Czochralski silicon wafer was scribed to have a rectangular shape. The specimen was flexed under 4-point bending to produce a constant bending moment in the mid-portion of the plate. A known in-plane load P that simulates residual stresses was applied and the resulting interference pattern under different load levels (tensile and compressive) was recorded photographically.

The mid-point deflection and plate curvature was found to increase under compressive loads and decrease under tensile loads. This situation is depicted schematically in Fig. 3. A schematic of the top view of the silicon sample is given in Fig. 4 where the inner

load bearing pins of the 4-point bend apparatus (2-in span), the applied load P and moment M, the line along which the optical data were taken and the coordinate frame (x and y axes) are shown. The local deflection and curvature was found by analyzing the interference pattern and by using geometric scale factors (to determine the actual distances from the photographs). The interference pattern for five combinations of P and M are shown in Fig. 5. As can be visually identified, the relative positions and density of fringes vary with P and M.

ANALYSIS

(1) Determination of the Local Curvature From the Experimental Data

To find the local curvature of the silicon plate at an arbitrary point Q, 3-point method is used in conjunction with the optical data in the vicinity of point Q. Fig. 6 shows a small portion of the silicon plate which contains point Q at which optical information is gathered.

The radius of curvature of the silicon plate at point Q is obtained by passing a circle throught the data points which has the form

$$x^2 + z^2 + 2dx + 2ez + f = 0 \qquad (1)$$

and the radius of which can be expressed as

$$R = (d^2 + e^2 + f)^{1/2} \qquad (2)$$

where

d, e and f are constants to be determined.

After reducing the optical information at three solution stations

surrounding point Q we get

x_1 Z_1 at point 1 ,

x_2 Z_2 at point 2 and

x_3 Z_3 at point 3

Substituting these data into Eq. (1) we get.

$$2dx_1 + 2eZ_1 + f = -(x_1^2 + Z_1^2)$$

$$2dx_2 + 2eZ_2 + f = -(x_2^2 + Z_2^2)$$

$$2dx_3 + 2eZ_3 + f = -(x_3^2 + Z_3^2)$$

or in matrix form

$$\begin{bmatrix} x_1 & Z_1 & 1 \\ x_2 & Z_2 & 1 \\ x_3 & Z_3 & 1 \end{bmatrix} \begin{Bmatrix} 2d \\ 2e \\ f \end{Bmatrix} = - \begin{bmatrix} x_1^2 + Z_1^2 \\ x_2^2 + Z_2^2 \\ x_3^2 + Z_3^3 \end{bmatrix}$$

from which d, e and f can be evaluated to determine the local curvature R.

(2) Determination of R_o for a Given Bending Moment M and Axial Force P.

Fig. 7 shows a portion of the rectangular silicon plate under the applied loading. Assuming the maximum deflection to be less than the plate thickness, the radius of curvature of the convex surface at point Q can be written as

$$R_o = \frac{h}{2} + \frac{Ph^2 + Ebh^3}{12M'}$$

where h = plate thickness,

b = width,

E = Young's Modulus,

$M' = M - Pw_Q$

P = in plane axial load,

M = applied bending moment and

w_Q = deflection of silicon plate at point Q.

The radius of curvature at the midspan is then given as

$$R_o\Big|_{\text{ç}} = \frac{h}{2} + \frac{Ebh^3}{12(M-Pw_{max})} + \frac{Ph^2}{12\ (M-Pw_{max})}$$

RESULTS

The sensitivity of the technique is obtained by measuring w_{max}, obtaining R_o from the optical data, calculating P and finding the difference between the applied load and the experimentally computed load. The smallest in-plane load used was 1.982N which results in a stress of 77.24 kPa (10 psi). The results of the percent difference between the calculated and computed in-plane load for different loading conditions are given in Table I. The percent difference ranges from 0.036 to 8.26

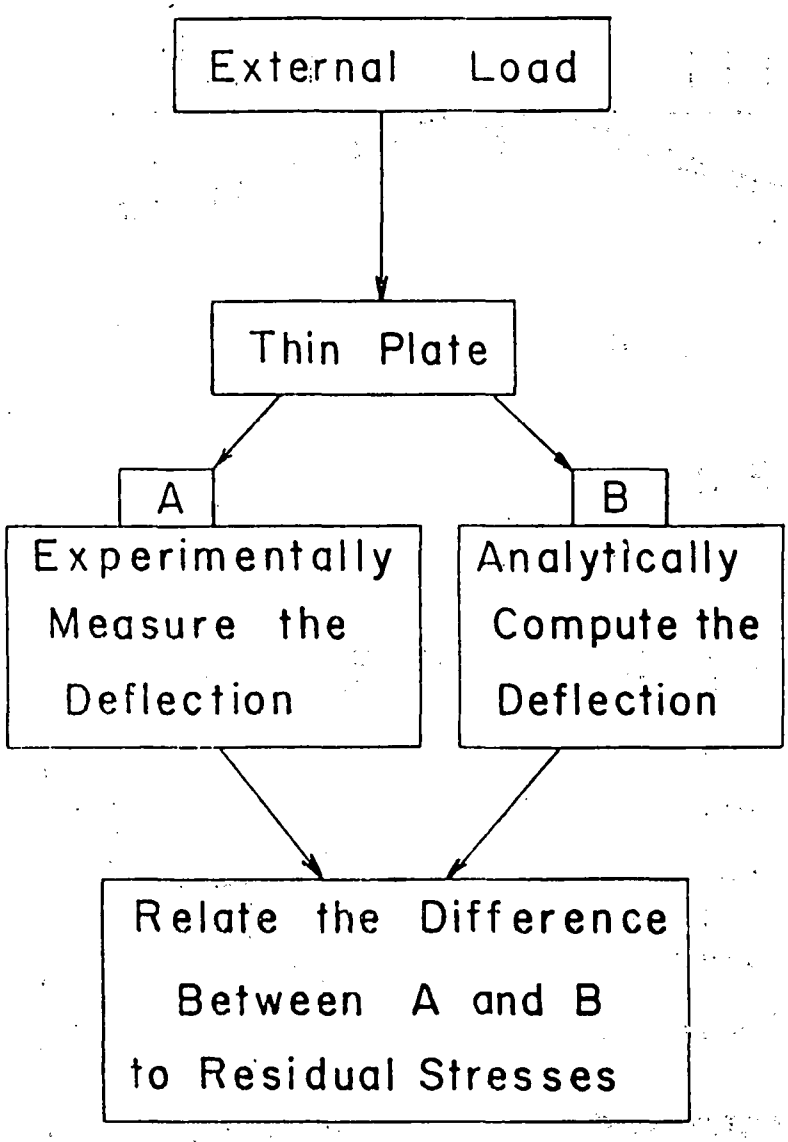
External Load
Thin Plate
A
B
Experimentally Measure the Deflection
Analytically Compute the Deflection
Relate the Difference Between A and B to Residual Stresses

Figure 1.

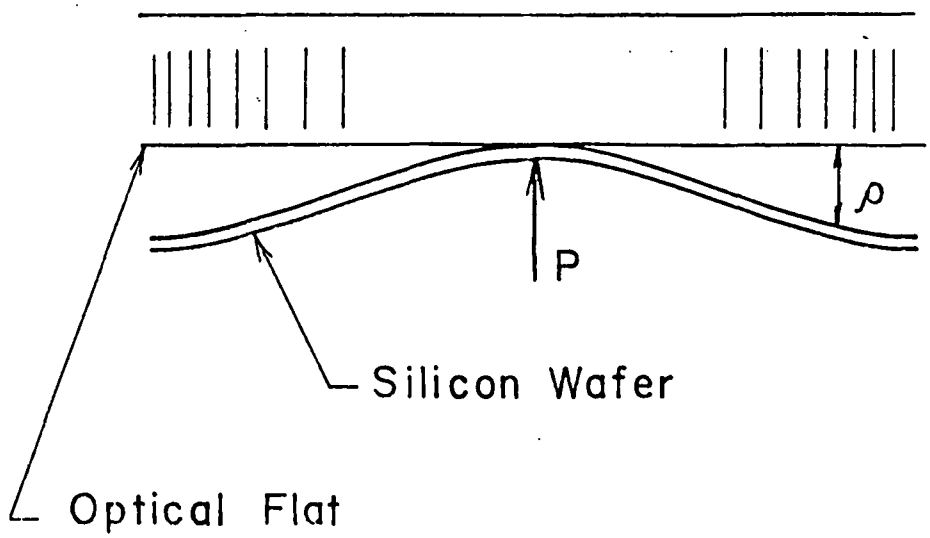

if $2\rho = (n - \frac{1}{2})\lambda$ if $2\rho = n\lambda$

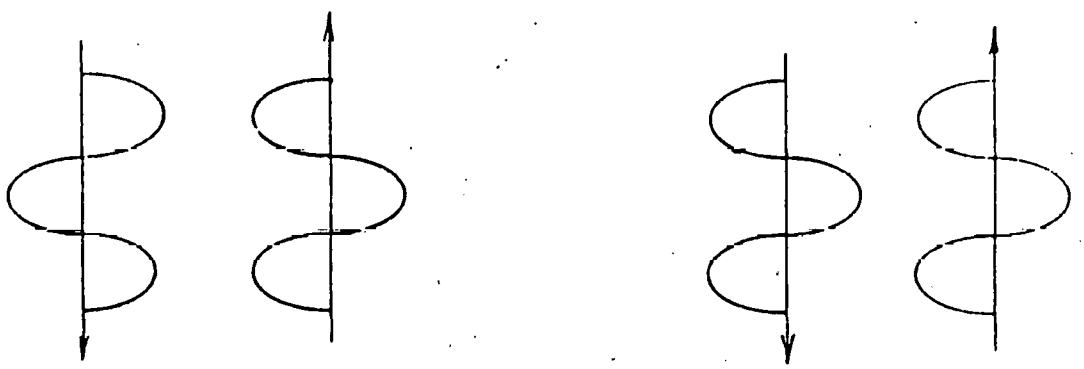

Dark Fringes

Destructive Interference

Light Fringes

Constructive Interference

Figure 2

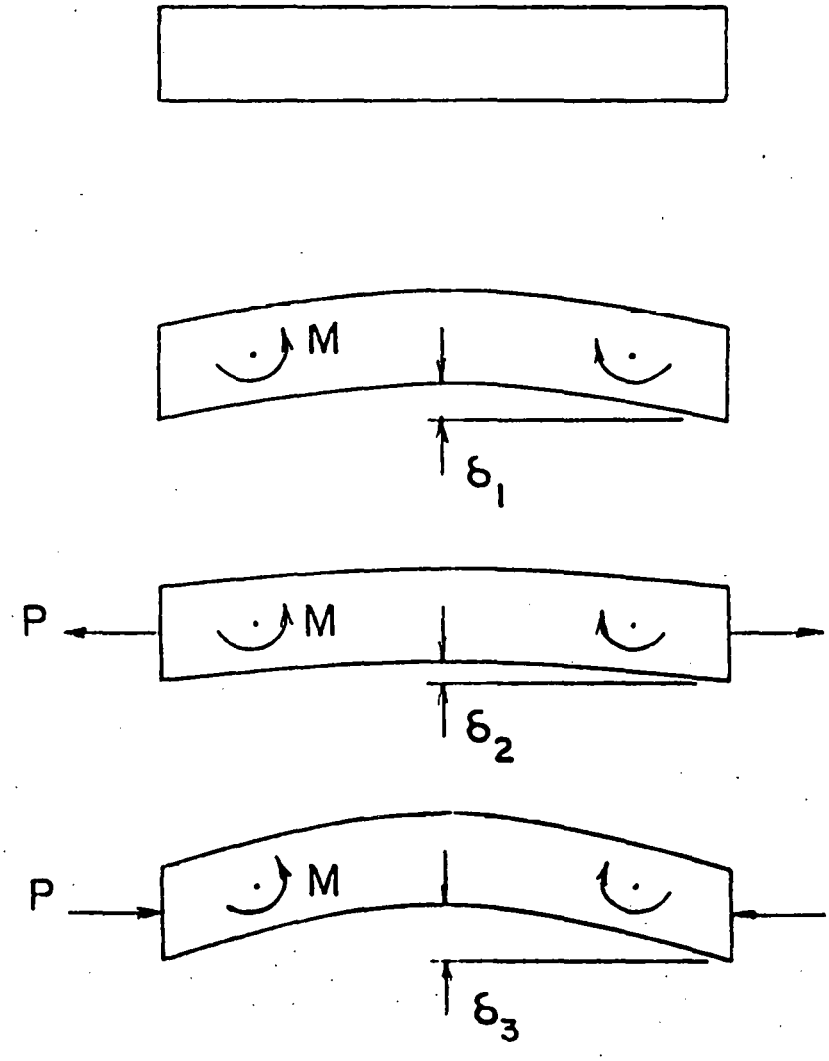

$$\delta_2 < \delta_1 < \delta_3$$

Figure 3.

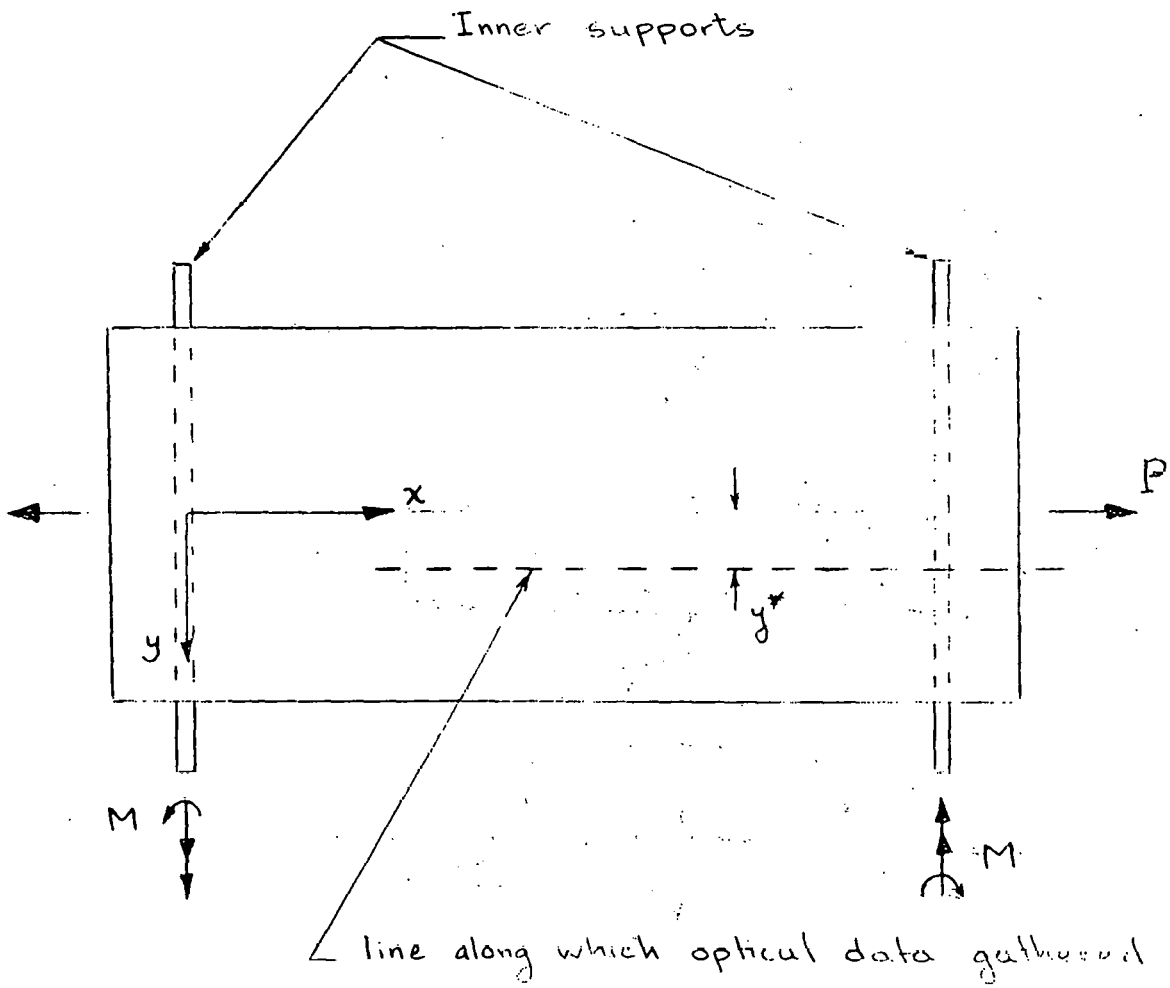
Inner supports
x
y
y*
P
M
M
line along which optical data gathered

Figure 4.

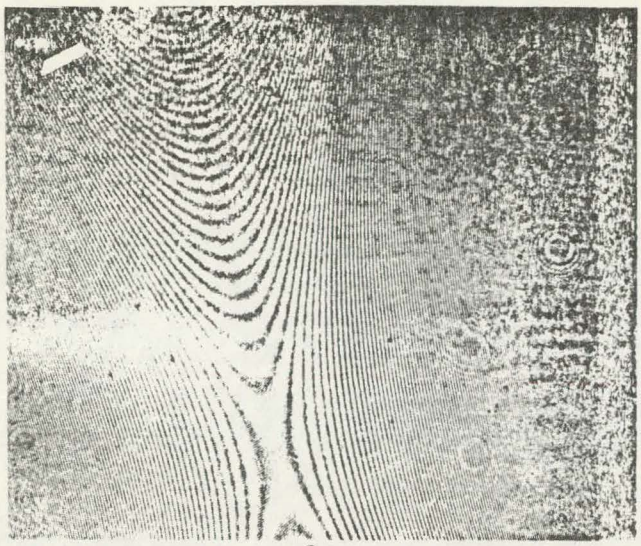

M= 0.02685 N.m^2 P = 0

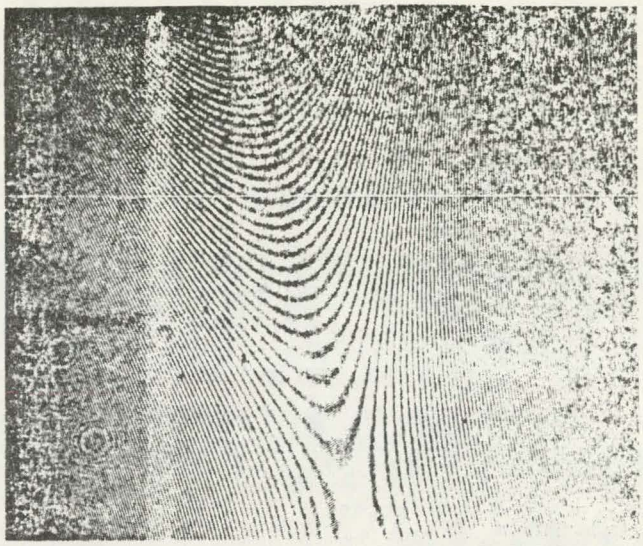

M = 0.02685 N.m^2 P = 1.962 N

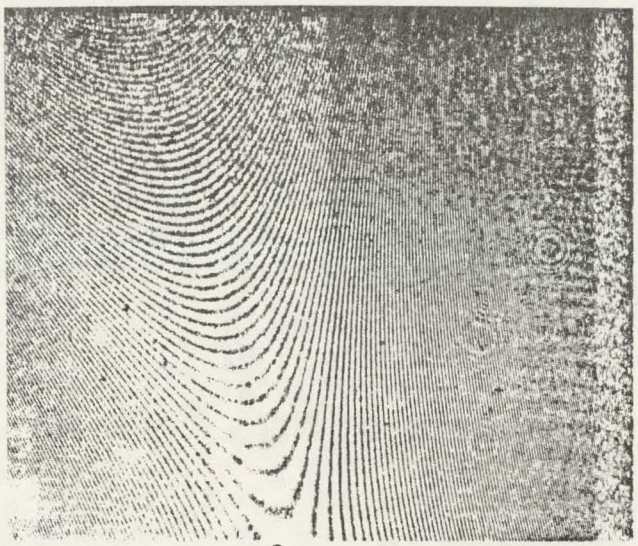

M = 0.02685 N.m^2 P = 3.934 N

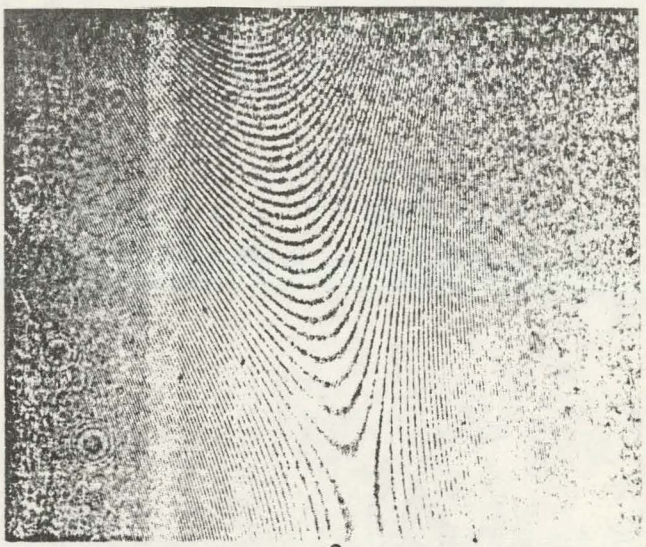

M = 0.0403 N.m^2 P = 3.924 N

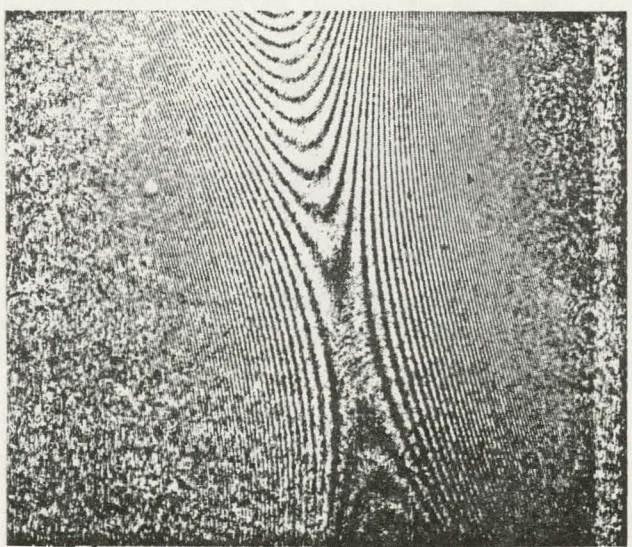

M = 0.0403 N.m^2 P = -1.962 N

Figure 5.

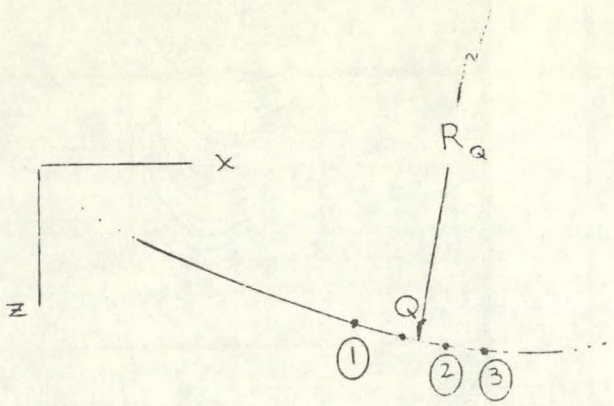

Figure 6.

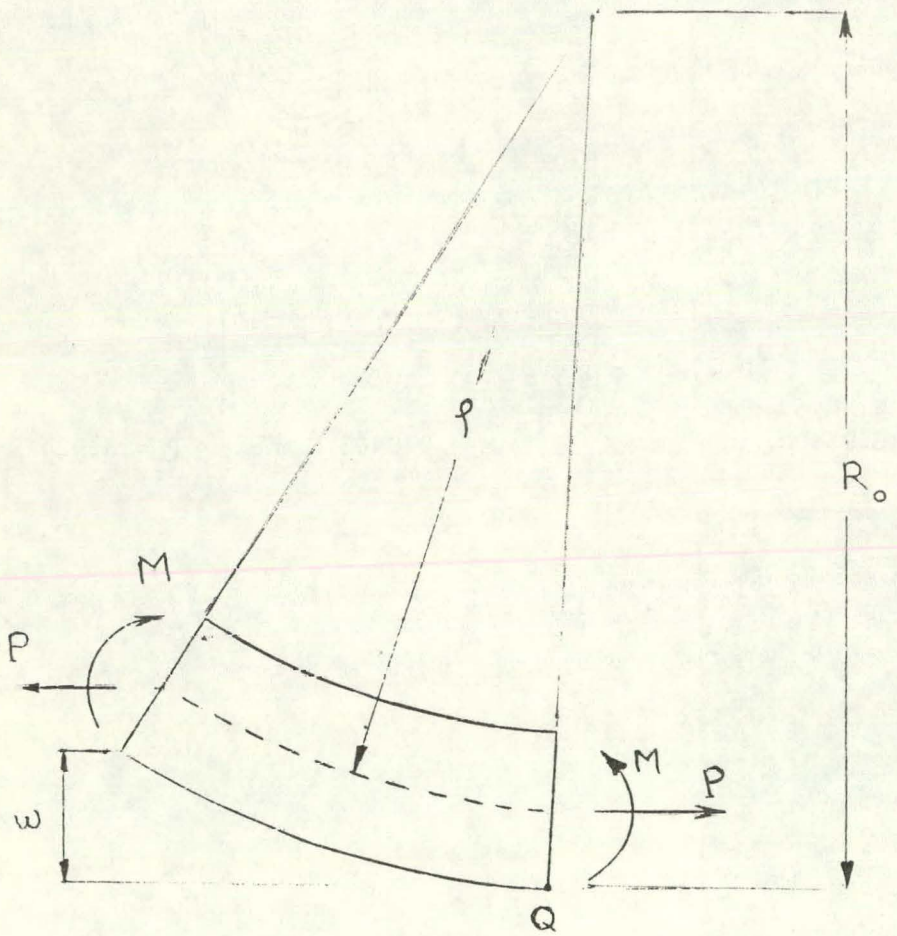

Figure 7.

w_{max} (m)	R_o (m) calculated from optical data	M ($N\text{-}m^2$) applied	P (N) applied	P (N) calculated	Difference %
$5x10^{-6}$	6.392	0.02685	0.		0.037 *
$5x10^{-6}$	6.3914	0.02685	1.962	1.8	8.26
$5x10^{-6}$	6.3938	0.02685	3.924	3.8	3.2
$7.6x10^{-6}$	4.2903	0.0403	3.924	3.82	2.7
$7.6x10^{-6}$	4.243	0.0403	-1.962	-1.88	4.2

* (percent difference calculated in bending moment M)

Table I. Percent difference between calculated and applied in-plane load , P , for a given bending moment M.

☆ U.S. GOVERNMENT PRINTING OFFICE: 1983—746-081/2123